Title	Room temperature ferroelectric and magnetic investigations and detailed phase analysis of Aurivillius phase Bi 5Ti 3Fe 0.7Co 0.3O 15 thin films
Authors	Keeney, Lynette;Kulkarni, Santosh;Deepak, Nitin;Schmidt, Michael;Petkov, Nikolay;Zhang, Panfeng F.;Cavill, Stuart;Roy, Saibal;Pemble, Martyn E.;Whatmore, Roger W.
Publication date	2012-09
Original Citation	Keeney, L., Santosh, K., Deepak, N., Schmidt, M., Petkov, N., Zhang, P. F., Cavill, S., Roy, S., Pemble, M. E. and Roger W. Whatmore (2012) ' Room temperature ferroelectric and magnetic investigations and detailed phase analysis of Aurivillius phase Bi 5Ti 3Fe 0.7Co 0.3O 15 thin films', Journal of Applied Physics, 112(5), 052010. http://dx.doi.org/10.1063/1.4745936
Type of publication	Article (peer-reviewed)
Link to publisher's version	10.1063/1.4745936
Rights	© 2012 American Institute of Physics. This article may be downloaded for personal use only. Any other use requires prior permission of the author and AIP Publishing. The following article appeared in L. Keeney et al. J. Appl. Phys. 112, 052010 (2012) and may be found at http://dx.doi.org/10.1063/1.4745936
Download date	2025-01-15 01:19:16
Item downloaded from	https://hdl.handle.net/10468/2989

Room temperature ferroelectric and magnetic investigations and detailed phase analysis of Aurivillius phase Bi5Ti3Fe0.7Co0.3O15 thin films

Lynette Keeney, Santosh Kulkarni, Nitin Deepak, Michael Schmidt, Nikolay Petkov et al.

Related Articles

Domain evolution in lead-free thin film piezoelectric ceramics
J. Appl. Phys. 112, 052014 (2012)

Ferroelectric domain morphology and structure in Li-doped (K,Na)NbO3 ceramics
J. Appl. Phys. 112, 052005 (2012)

Electric field induced phase instability in typical (Na,K)(Nb,Sb)O3-LiTaO3 ceramics near orthorhombic and tetragonal phase boundary
Appl. Phys. Lett. 101, 092906 (2012)

Effects of Gd substitution on microstructures and low temperature dielectric relaxation behaviors of SrTiO3 ceramics
J. Appl. Phys. 112, 034114 (2012)

Resistive switching and threshold switching behaviors in La0.1Bi0.9Fe1−xCoxO3 ceramics
J. Appl. Phys. 112, 034110 (2012)

Additional information on J. Appl. Phys.

Journal Homepage: http://jap.aip.org/

Journal Information: http://jap.aip.org/about/about_the_journal

Top downloads: http://jap.aip.org/features/most_downloaded

Information for Authors: http://jap.aip.org/authors

Room temperature ferroelectric and magnetic investigations and detailed phase analysis of Aurivillius phase Bi$_5$Ti$_3$Fe$_{0.7}$Co$_{0.3}$O$_{15}$ thin films

Lynette Keeney,[1,a)] Santosh Kulkarni,[1] Nitin Deepak,[1] Michael Schmidt,[1]
Nikolay Petkov,[1] Panfeng F. Zhang,[1] Stuart Cavill,[2] Saibal Roy,[1] Martyn E. Pemble,[1]
and Roger W. Whatmore[1]

[1]*Tyndall National Institute, University College Cork, "Lee Maltings," Dyke Parade, Cork, Ireland*
[2]*Diamond Light Source Ltd., Harwell Science and Innovation Campus, Didcot, Oxfordshire OX11 0DE,
United Kingdom*

Aurivillius phase Bi$_5$Ti$_3$Fe$_{0.7}$Co$_{0.3}$O$_{15}$ (BTF7C3O) thin films on α-quartz substrates were fabricated by a chemical solution deposition method and the room temperature ferroelectric and magnetic properties of this candidate multiferroic were compared with those of thin films of Mn^{3+} substituted, Bi$_5$Ti$_3$Fe$_{0.7}$Mn$_{0.3}$O$_{15}$ (BTF7M3O). Vertical and lateral piezoresponse force microscopy (PFM) measurements of the films conclusively demonstrate that BTF7C3O and BTF7M3O thin films are piezoelectric and ferroelectric at room temperature, with the major polarization vector in the lateral plane of the films. No net magnetization was observed for the in-plane superconducting quantum interference device (SQUID) magnetometry measurements of BTF7M3O thin films. In contrast, SQUID measurements of the BTF7C3O films clearly demonstrated ferromagnetic behavior, with a remanent magnetization, B_r, of 6.37 emu/cm^3 (or 804 $m$emu/g), remanent moment = 4.99×10^{-5} emu. The BTF7C3O films were scrutinized by x-ray diffraction, high resolution transmission electron microscopy, scanning transmission electron microscopy, and energy dispersive x-ray analysis mapping to assess the prospect of the observed multiferroic properties being intrinsic to the main phase. The results of extensive micro-structural phase analysis demonstrated that the BTF7C3O films comprised of a 3.95% Fe/Co-rich spinel phase, likely CoFe$_{2-x}$Ti$_x$O$_4$, which would account for the observed magnetic moment in the films. Additionally, x-ray magnetic circular dichroism photoemission electron microscopy (XMCD-PEEM) imaging confirmed that the majority of magnetic response arises from the Fe sites of Fe/Co-rich spinel phase inclusions. While the magnetic contribution from the main phase could not be determined by the XMCD-PEEM images, these data however imply that the Bi$_5$Ti$_3$Fe$_{0.7}$Co$_{0.3}$O$_{15}$ thin films are likely not single phase multiferroics at room temperature. The PFM results presented demonstrate that the naturally 2D nanostructured Bi$_5$Ti$_3$Fe$_{0.7}$Co$_{0.3}$O$_{15}$ phase is a novel ferroelectric and has potential commercial applications in high temperature piezoelectric and ferroelectric memory technologies. The implications for the conclusive demonstration of ferroelectric and ferromagnetic properties in single-phase materials of this type are discussed. © *2012 American Institute of Physics.* [http://dx.doi.org/10.1063/1.4745936]

I. INTRODUCTION

The magnetoelectric effect—the coupling of magnetisation to an electric field, or polarization to a magnetic field, is of considerable interest, both for the basic science involved and for a range of potential devices. While the effect was first seen in single phase materials such as Cr$_2$O$_{3,}$[1] so far the largest effects have been observed in composite materials, such as PMN-PT (0.7Pb(Mg$_{1/3}$Nb$_{2/3}$)O$_3$-0.3PbTiO$_3$)/ Terfenol-D laminates.[2] Magnetoelectric multiferroic materials,[3] in which ferroelectric and magnetic order parameters are coupled such that switching one switches the other, are of considerable interest for potential applications such as spin based memory/logic devices.[4] However, these materials are unusual, and while there are a few examples which show the effect at low temperature, such as ferroelectric, antiferro-

magnetic nickel iodine boracite,[5] there is only one which shows this effect at room temperature: BiFeO$_3$, which is ferroelectric and antiferromagnetic, and thus cannot be switched by a magnetic field.[6] So far, there are no confirmed room-temperature ferroelectric/ferromagnetics demonstrating magnetoelectric coupling.

The Aurivillius[7] bismuth-based ferroelectrics are 2D layer-structured materials with a large c-axis lattice parameter, in the nanometer range. The compounds are described by the general formula Bi$_2$O$_2$ ($A_{m-1}B_m$O$_{3m+1}$). The unit cells consist of (Bi$_2$O$_2$)$^{2+}$ layers lying in the (001) plane, which alternate with mABO$_3$ perovskite units. On increasing the number of perovskite layers (m), the micro-structural, magnetic, and physical properties of the materials can be altered significantly.[8] Additionally, the mABO$_3$ perovskite blocks can accommodate a wide range of metal ions with +3 to +5 oxidation states[9,10] where chemical substitution has been used to effect enhancements to the electrical properties of the materials.[11,12]

Hill[13] has suggested that the conditions for obtaining ferroelectricity and ferromagnetism in a single phase can potentially be met by incorporating d^0 and d^n cations into the same structure. So far, this has not been achieved in simple perovskites. However, the possibility exists that this might be achieved by introducing magnetic cations into ferroelectric Aurivillius layer-structures. A number of researchers have investigated a wide range of discrete compositions as bulk ceramics in the $(BiFeO_3)nBi_4Ti_3O_{12}$ system,[14,15] and while many of these are ferroelectric, no conclusive evidence has been found for ferromagnetic behaviour.

Piezoresponse force microscopy (PFM) has emerged as a powerful technique for locally probing nanoscale phenomena in piezoelectric and ferroelectric materials on the nanometer scale[16,17] and has been used to identify the $m = 4$ $Bi_5Ti_3FeO_{15}$ and $Bi_5Ti_3Fe_{0.7}Mn_{0.3}O_{15}$ thin films as novel ferroelectric phases.[18] However, these films do not demonstrate ferromagnetic hysteresis at room temperature.[19] Ferroelectric properties have also been demonstrated for the Co^{3+} substituted $m = 4$ Aurivillius phase thin films, $Bi_5Fe_{0.75-}Co_{0.25}Ti_3O_{15}$, by macroscopic ferroelectric test systems.[20] Recently, the coexistence of ferroelectricity and ferromagnetism above room temperature has been reported in $Bi_5Ti_3-Fe_{0.5}Co_{0.5}O_{15}$ ceramics.[21] While it was clear from the x-ray diffraction (XRD) data reported in this work that the ceramics were apparently single-phase Aurivillius compounds, neither did it report any micro-structural analysis of the ceramics nor did it put any upper-bound estimates on any possible magnetic phases (such as spinels) which might have been present at low levels.

In this study, we report the first magnetic investigations of $Bi_5Ti_3Fe_{0.7}Co_{0.3}O_{15}$ (BTF7C3O) thin films on quartz prepared by a chemical solution deposition method. The local electromechanical properties of the BTF7C3O thin films have been investigated for the first time by PFM. The room temperature ferroelectric and magnetic properties of this candidate multiferroic are compared with those of thin films of Mn^{3+} substituted, $Bi_5Ti_3Fe_{0.7}Mn_{0.3}O_{15}$. The results of careful XRD and high resolution transmission electron microscopy (HRTEM)/scanning transmission electron microscopy (STEM) phase analysis are described and the prospect of the observed multiferroic properties being intrinsic to the main $Bi_5Ti_3Fe_{0.7}Co_{0.3}O_{15}$ phase is assessed in conjunction with x-ray magnetic circular dichroism photoemission electron microscopy (XMCD-PEEM) imaging. X-ray absorption spectroscopy (XAS) and XMCD images were processed using PEEM image microscopy manipulation (PIMM) analysis routines.[22]

II. EXPERIMENTAL

Solutions of $Bi_5Ti_3Fe_{0.7}Mn_{0.3}O_{15}$ (BTF7M3O) and $Bi_5Ti_3Fe_{0.7}Co_{0.3}O_{15}$ (BTF7C3O) were prepared by dissolving the required amounts of $Bi(NO_3)_3 \cdot 5H_2O$ and $Ti(OCH_2CH_2CH_2CH_3)_4$ (titanium(IV) butoxide) in lactic acid at room temperature. $Fe(NO_3)_3 \cdot 9H_2O$ and $Mn(C_5H_7O_2)_3$ (manganese(III) acetylacetonate) or $Co(C_5H_7O_2)_3$ (cobalt(III) acetylacetonate), as appropriate, were dissolved separately in acetylacteone. When complete dissolution was

achieved, the Fe^{3+}/Mn^{3+} or Fe^{3+}/Co^{3+} solution was slowly dropped into the Bi^{3+}/Ti^{4+} solution under constant stirring to prepare 0.075 mol dm^{-3} solutions. For all solutions, 17.5 mol. % excess bismuth was used to compensate for evaporation of bismuth during the annealing process.[19] The films were spin-coated on α-quartz substrates (42.75 ± 15'ST-Cut) by a commercial spinner (spin coater KW-4A, Chemat Technology) operating at 4500 rpm for 30 s. Quartz substrates (350 μm thick) were chosen for their low diamagnetic contribution. Excess solvents and residual organics were removed from the films by baking on a calibrated hot plate at 300 ± 5 °C for approximately 10 min. Each individual deposition yielded films of approximately 100 nm in thickness and the deposition process was repeated until film thicknesses close to 500 nm were achieved, as observed from cross-section scanning electron microscopy (SEM) measurements. The films were annealed in ambient air for 1 h in a conventional furnace at temperatures of 800 °C (BTF7M3O films) or 850 °C (BTF7C3O films).

XRD profiles were recorded at room temperature using a Philips Xpert PW3719 MPD diffractometer, equipped with a Cu-Kα radiation source (40 kV and 35 mA) and a nickel filter on the incident beam over the range $5° \leq 2\theta \leq 37.5°$. Restricted range slow speed scans were recorded using an X'pert PRO PANalytical XRD equipped with a Cu-Kα radiation source (45 kV and 40 mA) where the incident beam was filtered with an x-ray mirror and the diffracted beam was filtered using a monochromator.

Topography was examined using high resolution scanning electron microscopy (HRSEM) and atomic force microscopy (AFM). SEM images and energy dispersive x-ray (EDX) analysis spectra were obtained using a FEI Quanta 630 high resolution scanning electron microscope. A commercial atomic force microscope (MFP-3D^{TM}, Asylum Research) in AC mode was used for topography mapping of the films. Olympus AC160TS silicon cantilevers (Al reflex coated, ~300 kHz resonant frequency) were used for imaging. Cross-sections of the BTF7C3O thin films were prepared for micro-structural analysis using a FEI DualBeam Helios NanoLab 600i focussed ion beam (FIB) (final thinning at 93 pA 30 kV, final polish 2 kV 28 pA). Microstructural analysis was performed on the BTF7C3O films using HRTEM (Jeol 2100 transmission electron microscope; 200 kV; double tilt holder) in conjunction with selected area electron diffraction (SAED) and EDX analysis (medium spot size, x-ray generation area 20–30 nm in diameter, 30–50 nm thickness). Note that normally ~10% error should be accounted for when calculating d-spacings from SAED due to electron optics of the instrumentation. Elemental mapping using EDX over larger sample areas (12–15.5 μm^2) was performed using the STEM mode at the FEI Helios Nanolab.

Electromechanical responses of the films were measured by PFM using an Asylum Research MFP-3D^{TM} AFM in contact mode equipped with a HVA220 Amplifier for PFM. Out-of-plane electromechanical responses of the films were investigated by single frequency and dual AC resonance tracking piezoresponse force microscopy (DART-PFM)[23] modes. In-plane electromechanical responses were imaged using the single frequency lateral PFM mode (conducted at a

drive frequency of 100 kHz). Vertical DART-PFM hysteresis loop measurements were obtained by switching spectroscopy PFM (SS-PFM).[24–26] Olympus AC240TM Electrilevers, Ti/Pt coated silicon cantilevers (Al reflex coated, 70 kHz resonant frequency, $\sim$320 kHz contact resonance frequency) were used for PFM imaging.

Room temperature magnetic measurements of the thin films were carried out using a Quantum Design superconducting quantum interference device (SQUID) magnetometer (Quantum Design USA; Model—MPMS XL5) over an applied magnetic field range of $\pm$50 000 Oe. The diamagnetic contribution from the quartz substrate was subtracted from the magnetic measurements. The film weight was estimated from sample area and film thickness measurements (determined from HRSEM measurements), combined with the x-ray density to be 7.87×10^{-5} g and 7.23×10^{-5} g for BTF7M3O and BTF7C3O, respectively.

XAS and XMCD combined with spatially resolved PEEM imaging was carried out using the I06 Nanoscience beamline at the Diamond Light Source, UK synchrotron facility. Element specific images were acquired at the Fe, Co, Ti, and O L-edge resonances for right and left circularly polarized x-rays, respectively. Magnetic features were determined using XMCD as the contrast mechanism and, when

used in conjunction with XAS, the chemical states of the magnetic features ascertained.

III. RESULTS AND DISCUSSION

A. Thin film crystallinity and morphology

XRD patterns of the films are shown in Fig. 1(a) for BTF7M3O and Fig. 1(b) for BTF7C3O. The XRD scans reveal that both samples are pyrochlore-free, $m = 4$ Aurivillius phase thin films (Joint Committee for Powder Diffraction Standard (JCPDS) No. 38-1257). The lattice parameters for these were determined to be $a = 5.465$, $b = 5.362$, and $c = 42.260$ Å for BTF7M3O and $a = 5.474$, $b = 5.259$, and $c = 43.370$ Å for BTF7C3O. Particular care was taken in this study to assess the possibility of there being ferromagnetic second phases in the BTF7C3O thin films; as such phases might confuse the unequivocal detection of ferromagnetic hysteresis in the BTF7C3O phase. Hence, restricted scans were performed through the 2-theta region of BTF7C3O where XRD peaks signifying the presence of the ferromagnetic spinel impurity phases Fe_3O_4 or $CoFe_2O_4$ would be expected to be revealed, if present. These are the (311) reflections which are generally the most intense for the spinel phase and occur at $2\theta \sim 35.4°$. XRD patterns for BTF7C3O

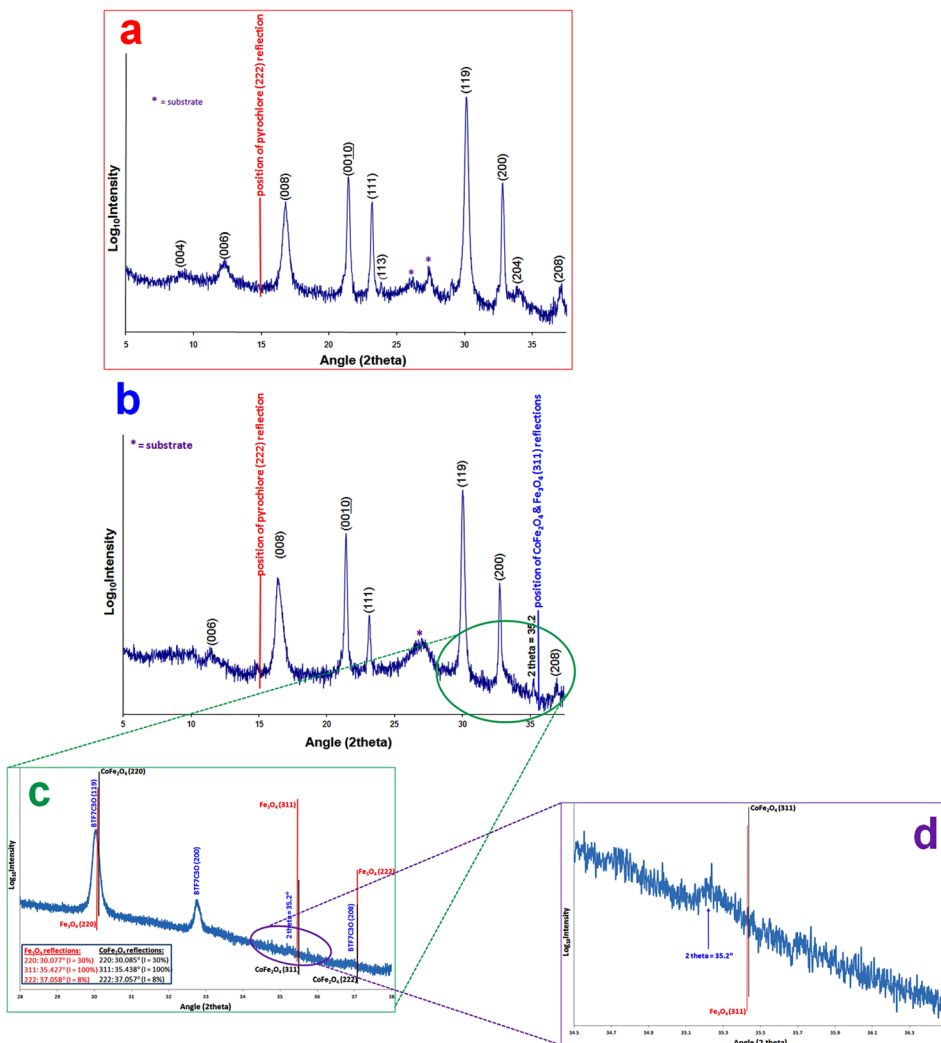FIG. 1. X-ray diffraction patterns of (a) $Bi_5Ti_3Fe_{0.7}Mn_{0.3}O_{15}$ and (b) $Bi_5Ti_3Fe_{0.7}Co_{0.3}O_{15}$ thin films on quartz substrates. The insets in (c) and (d) show restricted range slow speed scans through the 2-theta region which would be expected to reveal the presence of the ferromagnetic spinel impurity phases Fe_3O_4 or $CoFe_2O_4$, if present.

over the range range $28.5° \leq 2\theta \leq 36.5°$ (scan step size = 0.015°; time per step = 100 s) and over the range $34.5° \leq 2\theta \leq 36.5°$ (scan step size = 0.002°; time per step = 100 s) are shown in Figs. 1(c) and 1(d), respectively. The presence of a peak at 35.4° could not be identified from the restricted range XRD scans. Although spinel impurity phases are not immediately obvious from the XRD patterns, a small peak, with intensity very close to the noise level and a slightly larger d-spacing (2.54 Å; 2 theta = 35.2°) in the vicinity of the position if the (311) spinel reflection was noted. Given the possibility of an in-built linear strain of ca. 0.6% between the spinel phase and main BTF7C3O phase or between the spinel phase and substrate, the position of the (311) reflection could shift to 35.2°. In addition, since the (220) spinel reflection occurs at ~30.1°, this may be present but would be indistinguishable from the overlapping BTF7C3O (119) reflection. Such restricted XRD experiments alone cannot confirm the absence or presence of impurity spinel phases in the BTF7C3O thin films.

SEM and AFM measurements images reveal randomly oriented layered phases crystallised in plate-like morphologies characteristic of the Aurivillius type as shown in Figs. 2(a) and 2(b) for BTF7C3O. SEM-EDX measurements confirmed the stoichiometry of the films (Fig. 2(c)).

HRTEM analysis demonstrates that the BTF7C3O films on quartz consist of randomly oriented plate-like crystals with an underlying amorphous layer at the substrate interface (Figs. 3(a) and 3(b)). Microstructure assessment of the BTF7C3O grains (Figs. 3(c) and 3(d)) displays distinct grain

morphologies with high order reflections of the four-layered Aurivillius phase. Localized elemental mapping over several areas of the film using EDX indicated that the crystalline structures contain Bi, Ti, Fe, and Co, whereas the amorphous layer evidently consists of Bi and Si/SiO_2 (Fig. 4). Given that excess bismuth was used in the synthetic process, it is likely that at the processing conditions used for crystallizing the main phase (850 °C), a reaction between Bi_2O_3 and SiO_2 occurred at the interface between the film and substrate to form an amorphous Bi_2O_3-SiO_2 phase (e.g., $Bi_{12}SiO_{20}$, $Bi_4Si_3O_{12}$, Bi_2SiO_5)[27–30] on cooling. No evidence of Fe/Co-rich/Bi poor areas were detected in the BF7C3O film at the resolution of the localized HRTEM-EDX maps (Fig. 4), however, there is always the risk that impurities are not homogeneously distributed throughout the sample and therefore localized elemental mapping (frame of view is 400 nm) may not give a true representation of the whole BTF7C3O sample.

B. Local room temperature ferroelectric investigations

PFM (Refs. 23, 25, and 31–34) was used to investigate the local electromechanical properties of the films at room temperature. Vertical and lateral single frequency measurements were conducted at a drive frequency of 100 kHz (Fig. 5). These images demonstrate that the films are piezoelectric at room temperature, with the major polarization vector in the lateral plane of the films, since the absolute piezoresponses in the lateral direction (0.09 pm/V for B7TF3O
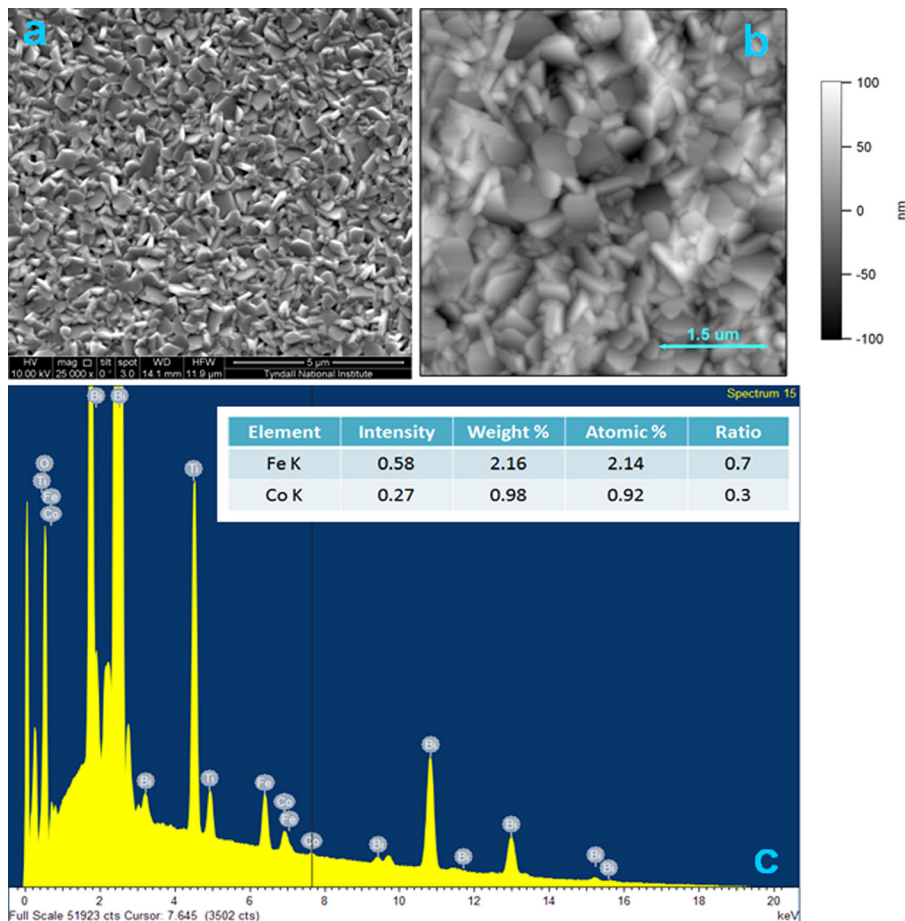

Element	Intensity	Weight %	Atomic %	Ratio
Fe K	0.58	2.16	2.14	0.7
Co K	0.27	0.98	0.92	0.3

FIG. 2. Representative (a) SEM image, (b) AFM image, and (c) SEM-EDX data for Bi_5Ti_3-$Fe_{0.7}Co_{0.3}O_{15}$ thin film topography on quartz substrate.
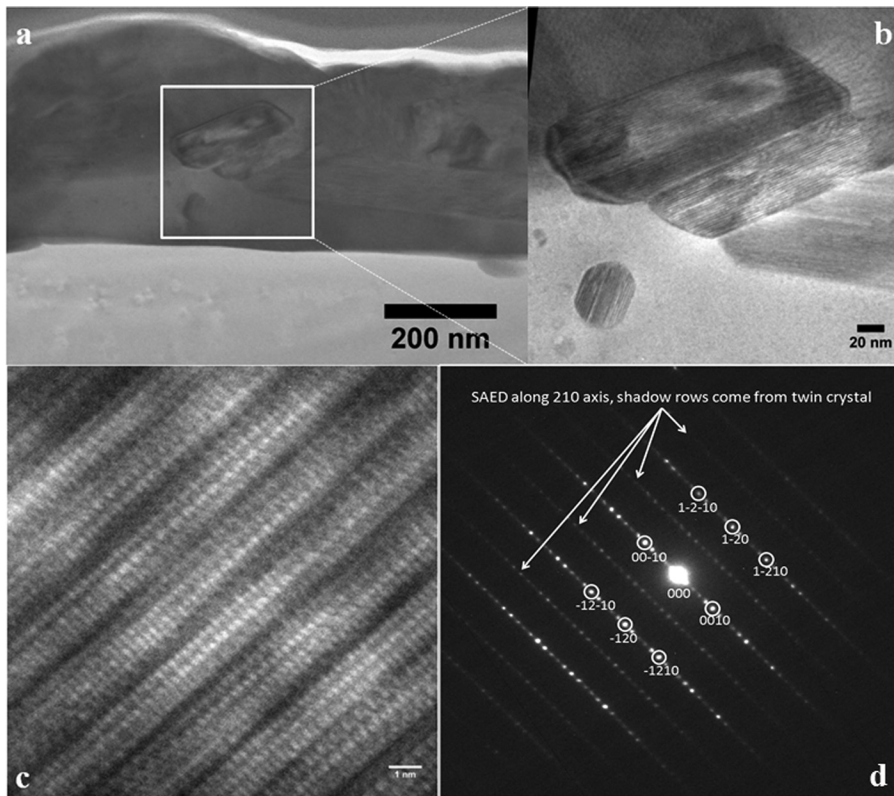
FIG. 3. (a) Representative HRTEM microstructural analysis image of a cross-section of BTF7C3O on quartz. (b) Magnified HRTEM image of box in "(a)." (c) HRTEM image of Aurivillius phase grain. (d) SAED pattern of Aurivillius phase grain.

and 0.13 pm/V for B7TF3O) are higher than those measured for the vertical direction (0.06 pm/V and 0.04 pm/V). As the B7TFM3O and BTF7C3O thin films are preferentially c-axis oriented (Fig. 1), most of the grains have their crystallographic a-axis lying in the lateral plane of the film. The major polarization vector for Aurivillius phase materials with even numbers of perovskite layers is along the a-axis[35] and therefore perpendicular to the applied field in vertical PFM. As a result, c-axis oriented grains would not contribute to a vertical PFM response and the lateral PFM images overall demonstrate greater piezoresponses than the vertical PFM images. Since the films are comprised of some a-axis oriented grains as well as c-axis oriented grains (for instance, the relative intensity of the (200) reflection in BTF7C3O is 30.3% (Fig. 1)), vertical PFM response appears to arise from a-axis oriented grains. These grains have their crystallographic a-axis tilted out-of-plane and are therefore accessible to probing by vertical PFM. Domains (circled in the PFM amplitude images in Fig. 5) showing high out-of-plane response, demonstrate weak in-plane response and vice versa in the BTF7M3O films. The same observation was noted for the BTF7C3O films. However, the vertical piezoresponse was slightly weaker when compared with the BTF7M3O films.

Vertical DART-PFM switching spectroscopy-PFM[23–26,36] measurements in the presence and absence of an applied DC bias were used to investigate local room temperature ferroelectric switching behaviour (180°) in the films; loops in the absence of an applied DC bias are presented in Fig. 6. The topography of the BTF7C3O sample captured during switching spectroscopy measurements is displayed in the inset in Fig. 6(c) and demonstrates where the PFM loop hysteresis

loop was taken for the B7TFC3O sample. The red spot indicates the PFM tip location, which probed the a-axis of the orthorhombic Aurivillius phase grain. Flat, c-axis oriented
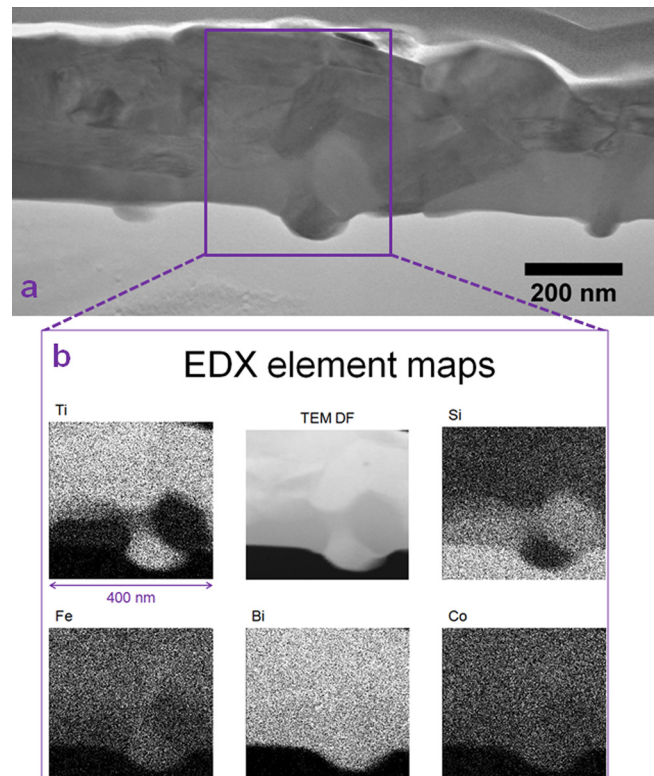

FIG. 4. Representative (a) TEM bright field image and (b) TEM dark field (DF) image with EDX elemental mapping of a cross section of BTF7C3O on quartz.
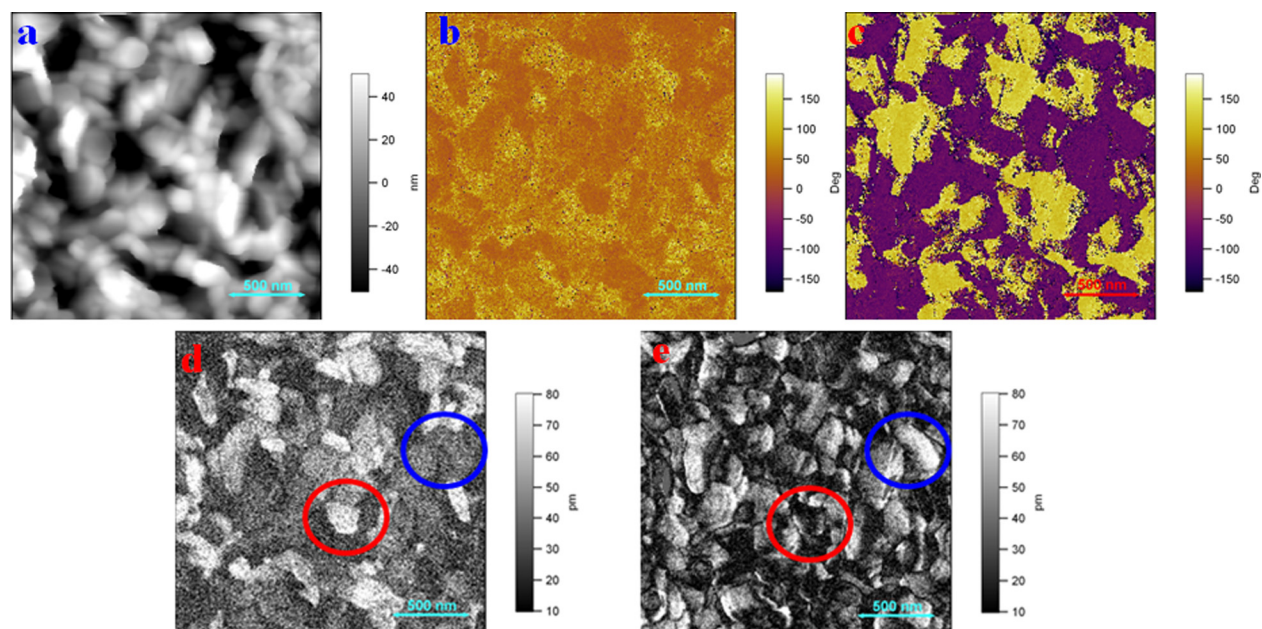
FIG. 5. (a) Topography, (b) vertical PFM phase, (c) lateral PFM phase, (d) vertical PFM amplitude, and (e) lateral PFM amplitude images of Bi_5Ti_3-$Fe_{0.7}Mn_{0.3}O_{15}$ thin film on quartz. Domains (circled in the PFM amplitude images) showing high out-of-plane response, demonstrate weak in-plane response and vice versa.

grains in the BTF7M3O and BTF7C3O thin films did not display vertical hysteresis, while tilted (*a*-axis oriented) grains clearly exhibited 180° ferroelectric switching. A higher applied bias (82.5 V/ ∼ 100 V/μm) is required for the probing wave form to switch BTF7C3O films out-of-plane, compared to that of the BTF7M3O (20.57 V/ ∼ 30 V/μm) analogues on quartz.

C. Room temperature magnetic investigations

Room temperature magnetic measurements of the BTF7M3O and BTF7C3O thin films on quartz were carried out using SQUID magnetometery. No net magnetization was observed for the in-plane SQUID measurements of BTF7M3O thin films on quartz. By contrast, the in-plane room temperature magnetization (M) vs. applied magnetic field (H) measurements of BTF7C3O thin films on quartz (Fig. 7) clearly demonstrated ferromagnetic behavior, with a

remanent moment of 4.99×10^{-5} emu and remanent magnetization, B_r, of 6.37 emu/cm^3 (or 804 $m$emu/g). The magnetization at 50 000 Oe was 22.4 emu/cm^3 (or 2.83 emu/g) and coercivity, H_c, of 1500 Oe. The remanent magnetization for BTF7C3O is about 103 times larger than the value ($B_r = 7.8$ $m$emu/g, H_c ∼410 Oe) reported for the $Bi_5Ti_3Fe_{0.5}$-$Co_{0.5}O_{15}$ ceramic by Mao *et al.*[21]

D. Detailed magnetic phase analysis

Trace amounts of second-phase inclusions could, if ferromagnetic, account for the observed magnetic response in the films (e.g., 2.8% of $CoFe_2O_4$—$B_r = 29.2$ emu/g (Ref. [37])—would give a remanent magnetization of 818 $m$emu/g (remanent moment of 5.13×10^{-5} emu)) and also could explain the increased magnetization value observed for the BTF7C3O thin films over the value reported for the Bi_5Ti_3-$Fe_{0.5}Co_{0.5}O_{15}$ ceramics.[21] As noted above, restricted
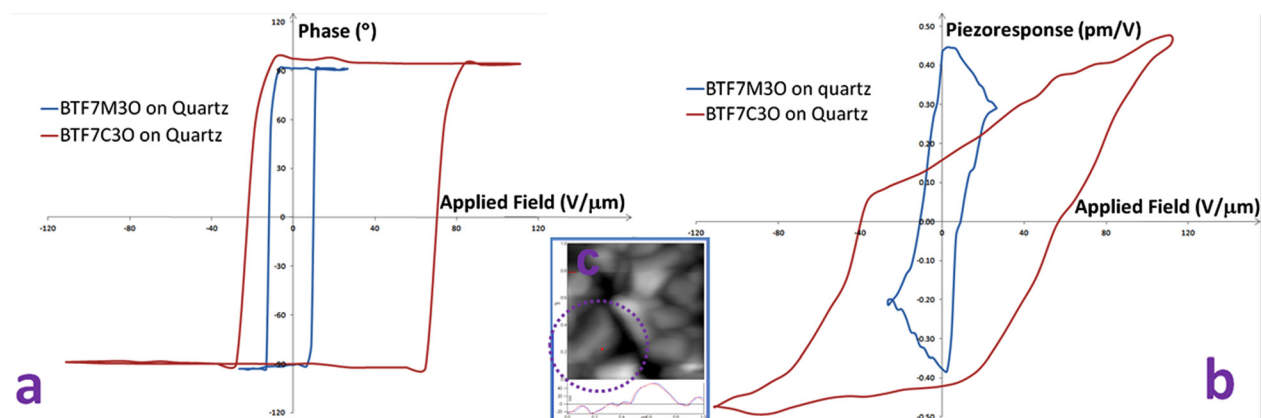

FIG. 6. Vertical DART-PFM switching spectroscopy (a) phase and (b) piezoresponse loops of $Bi_5Ti_3Fe_{0.7}Mn_{0.3}O_{15}$ and $Bi_5Ti_3Fe_{0.7}Co_{0.3}O_{15}$ thin films on quartz in the absence of an applied DC bias. Inset (c) demonstrates where the PFM loop hysteresis loop was taken for the B7TFC3O sample. The red spot indicates the PFM tip location.
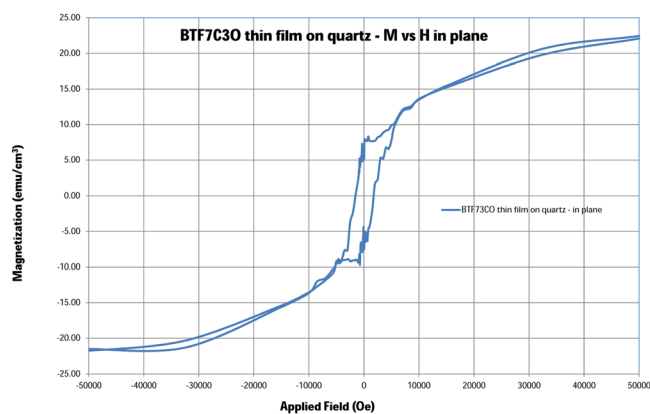
FIG. 7. In-plane room temperature in-plane M vs. H measurement of $Bi_5Ti_3Fe_{0.7}Co_{0.3}O_{15}$ thin film on quartz.

FIG. 8. STEM dark field image and EDX elemental mapping of (a) a 27 μm cross-section lamella and (b) a 29 μm cross-section lamella of BTF7C3O thin film on quartz.

XRD experiments and localized HRTEM-EDX mapping could not confirm the absence or presence of impurity spinel phases in the BTF7C3O thin films. Given that the presence of a small peak with a slightly larger d-spacing in the vicinity of the (311) spinel reflection was noted (Figs. 1(b)–1(d)), and that the observed magnetization value (804 $m$emu/g) was 103 times greater than that observed by Mao et. *al*. ($B_r = 7.8 \, m$emu/g, $H_c \sim 410 \, Oe$)[21] for the $Bi_5Ti_3Fe_{0.5}Co_{0.5}O_{15}$ ceramics, the BTF7C3O films deserve careful consideration and micro-structural phase analysis.

STEM with EDX mapping provides the capability of performing elemental mapping over larger cross-section areas to scrutinize the BTF7C3O thin film sample for possible Fe/Co-rich inclusions. This was conducted over a 27 μm cross-section (Fig. 8(a)) and a 29 μm cross-section (Fig. 8(b)) of two different BTF7C3O thin films, where it can be seen from the EDX elemental mapping that there is clear evidence of Fe/Co-rich/Bi poor inclusions. The inclusions also contained Ti. Due to imperfect mixing and exsolution during preparation, the inclusions in the sample shown in Fig. 8(a) are more homogeneously spread through the sample cross-section, whereas in the sample in Fig. 8(b), the inclusions are clustered together, with larger areas of the cross-section ($\sim$10 μm in length) where no inclusions could be detected. This demonstrates that detection of the magnetic clusters would be very difficult by localized HRTEM-EDX mapping (Fig. 4) and that the STEM-EDX mapping was an extremely effective technique for detecting trace amounts of impurity phases in our samples.

In order to determine whether the observed ferromagnetism (Fig. 7) in the BTF7C3O thin films originates from the $Bi_5Ti_3Fe_{0.7}Co_{0.3}O_{15}$ main phase or from the Fe/Co-rich inclusions, room temperature spatially resolved XAS and XMCD imaging was performed in conjunction with PEEM. Element specific images were acquired at the Fe and Co (Fig. 9) *L*-edge resonances for positive and negative circularly polarized x-rays. As with the STEM-EDX images, Fe and Co-rich inclusions can clearly be seen in the 6 μm XAS-PEEM images (Fig. 9(a) or Fig. 9(c)). From the XMCD-PEEM analysis ((Figs. 9(b) and 9(d)), it would seem that the magnetism arises from the Fe sites in the inclusions and that the Co present in the inclusions is not magnetic Co. PEEM
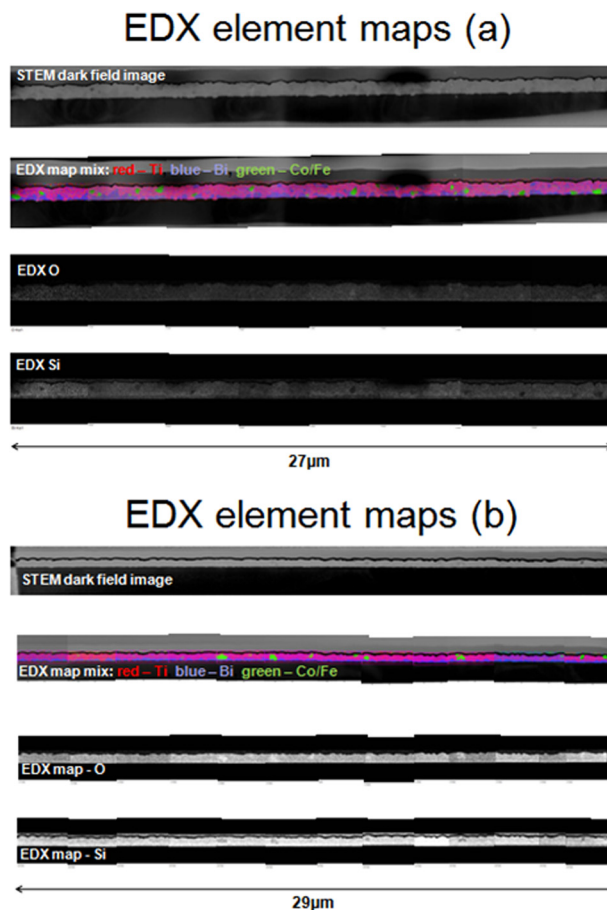
images measured at the Ti *L*-edge demonstrated that non-magnetic Ti was present over the course of the film. It is difficult to determine whether there is any magnetic response from the main $Bi_5Ti_3Fe_{0.7}Co_{0.3}O_{15}$ phase, as due to the relatively low Fe/Co content in the main phase, the XAS and XMCD data in the main phase appears as noise compared with the data from the Fe/Co-rich spinel phase inclusions, where the Fe/Co content is more concentrated. XMCD-PEEM imaging demonstrated that the majority of the observed magnetic response arises from the Fe/Co-rich spinel phase inclusions and is not intrinsic to the main $Bi_5Ti_3Fe_{0.7}Co_{0.3}O_{15}$ phase.

By conducting SAED patterns along the 211 zone axis of the Fe/Co-rich micro-structures (Fig. 10), and fitting the obtained *d*-spacings (d-sp) to the equation: $a(calc) = d^* (N)^{1/2}$ (where $N = h^2 + k^2 + l^2$), we find that the pattern fits with a $CoFe_{2-x}Ti_xO_4$ cubic spinel structure with a slightly larger lattice parameter (*a*) than that of $CoFe_2O_4$ (8.38 Å). It is likely that the Ti content of the phase influences the size of the unit cell, thereby increasing the lattice parameter of the spinel phase.[38]

The *d*-spacing of the (311) peak in the electron diffraction pattern of the Fe/Co-rich inclusions also matches with the peak at 2 theta = 35.2° noted in the x-ray diffraction pattern. We can thus calculate the spinel content of the BTF7C3O thin film by direct comparison of the integrated

SAED along 211 zone axis

11-3   1-1-1   1-31

02-2   000   0-22

-13-1   -111   -1-13

111, d-sp = 5.15 Å, a-calc = 8.92 Å
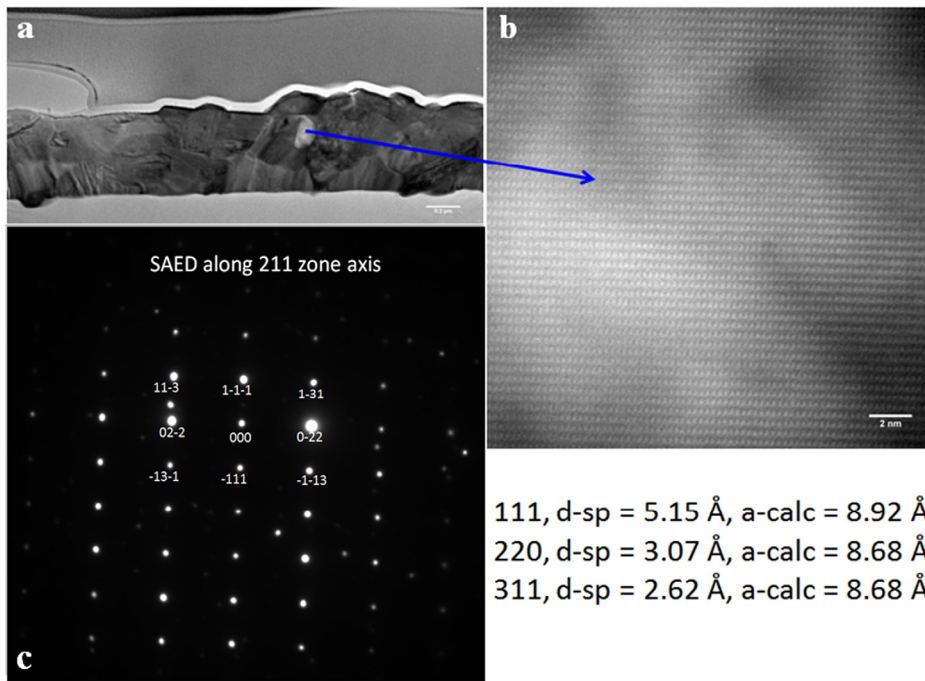220, d-sp = 3.07 Å, a-calc = 8.68 Å
311, d-sp = 2.62 Å, a-calc = 8.68 Å

FIG. 9. (a) Representative HRTEM cross-section image of BTF7C3O thin film on quartz, (b) magnified HRTEM image of Fe/Co-rich inclusion, and (c) SAED pattern of Fe/Co-rich inclusion.

intensity of the spinel (311) reflection in the x-ray diffraction pattern with the integrated intensity of the (200) reflection of the $Bi_5Ti_3Fe_{0.7}Co_{0.3}O_{15}$ phase, using the standard method for computing phase volume fractions.[39] Crystallographica[40] was used to compute the structure factors for the relevant reflections, based upon the atomic positions reported for $Bi_5Ti_3FeO_{15}$ (Ref. [41]) and the spinel phases.[42–44] We estimate on this basis that the volume fraction of the spinel phases in the BTF7C3O thin film detected by the XRD instrumentation is 1.22×10^{-2}.

However, there may be a portion of the impurity peak which is indistinguishable from the background noise of the XRD measurement. This could therefore introduce an error in the volume fraction calculations from the XRD instrumen-

tation and suggests a need for more sensitive phase analysis techniques. We used STEM with EDX mapping to put an upper-bound estimate on the Fe/Co-rich spinel phase (likely magnetic $CoFe_{2-x}Ti_xO_4$) present at low levels in the sample. STEM-EDX images demonstrated 23 inclusions over the $27\,\mu m$ lamella length (Fig. 8(a)) and 12 inclusions over the $29\,\mu m$ lamella length (Fig. 8(b)) with inclusion sizes ranging from $15\,nm$ to $1\,\mu m$. This gives an estimate of $3.9(\pm 0.3) \times 10^{-2}$ for the volume fraction of the Fe/Co-rich inclusions, a factor of three times the volume fraction calculated by the XRD method. Given that the STEM-EDX mapping method is a direct visual method and that instrumental factors such as x-ray absorption effects may influence the intensity of the XRD peak reflections, we assume that the
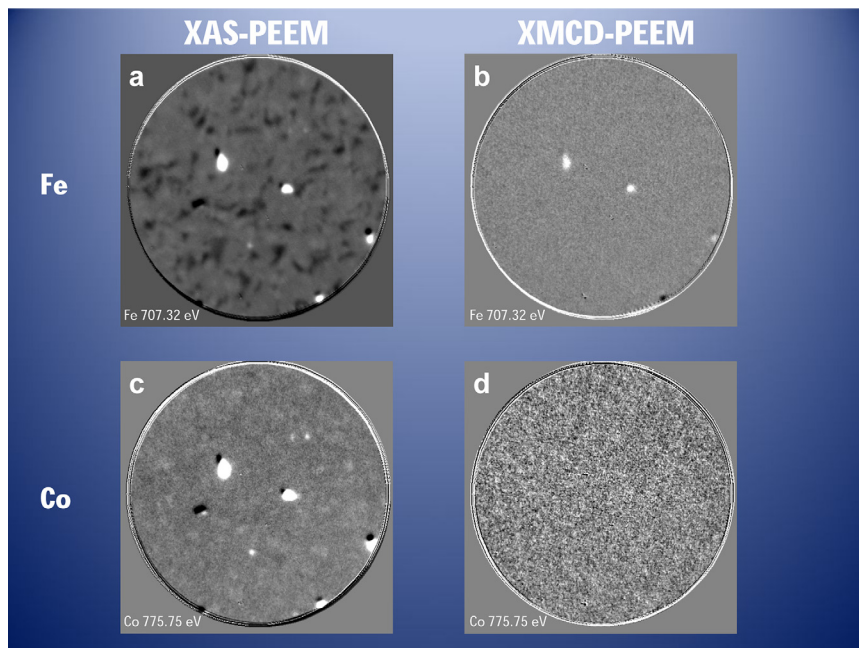

FIG. 10. (a) XAS-PEEM image at Fe *L*-edge resonance (707.32 eV) and (b) XMCD-PEEM image at Fe *L*-edge resonance (707.32 eV) demonstrating magnetic signature at the Fe edge for the Fe-rich inclusions. (c) XAS-PEEM image at Co *L*-edge resonance (775.75 eV) and (d) XMCD-PEEM image at Co *L*-edge resonance (775.75 eV) demonstrating no magnetic signature at the Co edge for the Co-rich inclusions. Frame of view is 6 μm.

volume fraction of the Fe/Co-rich spinel phase calculated by the STEM-EDX mapping technique is the more accurate value. Furthermore, an upper bound estimate should be used to determine the influence of magnetic inclusions on the observed magnetic moment of the BTF7C3O samples.

The presence of this magnetic titanium substituted $CoFe_2O_4$ phase at a volume fraction of 3.95% accounts for all of the observed magnetization in the BTF7C3O thin films. The detection of the magnetic impurities at this concentration was an arduous and lengthy task, as the inclusions were not always formed homogenously throughout the film; for example, there were sections of the films $\sim 10\,\mu m$ in length where Fe/Co-rich inclusions could not be detected. Thus, the ability to conduct EDX mapping over larger thin film lamellae sections in a raster using STEM was extremely valuable for our investigations. For samples with lower concentrations of impurities, their detection would be even more difficult. For instance, for samples to display the remanent magnetization value of BTF5C5O,[21] the volume of Co/Fe-rich impurities would have to be less than 0.02% to confirm that any of the observed ferromagnetism was intrinsic to the main Aurivillius phase. This would mean scanning sample cross-section lengths of 5.3 mm to detect this trace level of impurities by the STEM-EDX technique, even assuming no clumping-together of the impurity phase particles, which would be virtually impossible. Similarly, the detection of this level of second phase by XRD would be exceedingly difficult, if not impossible.

IV. CONCLUSIONS

We report the first PFM and SQUID magnetometry investigations of $Bi_5Ti_3Fe_{0.7}Co_{0.3}O_{15}$ thin films on quartz prepared by a chemical solution deposition method. The room temperature ferroelectric and magnetic properties of this candidate multiferroic were compared with those of thin films of Mn^{3+} substituted, $Bi_5Ti_3Fe_{0.7}Mn_{0.3}O_{15}$. The PFM imaging and reversible hysteresis loops demonstrate that the BTF7M3O and BTF7C3O thin films are conclusively ferroelectric with typical Aurivillius phase grain morphologies and response characteristics. BTF7M3O thin films are conclusively not ferromagnetic, whereas ferromagnetic hysteresis was observed in the SQUID magnetic measurements of the BTF7C3O thin films.

XMCD-PEEM imaging clearly confirms that the observed magnetic response arises from the Fe sites of inclusions of a $CoFe_{2-x}Ti_xO_4$-type phase, whereas a magnetic response from the main $Bi_5Ti_3Fe_{0.7}Co_{0.3}O_{15}$ phase was not evident. While the magnetic contribution from the main phase could not be determined by the XMCD-PEEM images, this data however implies that the $Bi_5Ti_3Fe_{0.7}Co_{0.3}O_{15}$ thin films are likely not single phase multiferroics at room temperature, as thorough phase and micro-structural analysis demonstrated the presence of magnetic $CoFe_{2-x}Ti_xO_4$ impurities at a volume fraction of 3.95%, which account for the entire measured magnetization in the BTF7C3O thin films. It is important to note that the kind of detailed analysis for possible magnetic impurity phases, and analysis of their effects, is generally absent from previous work reported on these types of materials.

The PFM analysis in this work has identified the $Bi_5Ti_{3-}Fe_{0.7}Mn_{0.3}O_{15}$ and $Bi_5Ti_3Fe_{0.7}Co_{0.3}O_{15}$ thin films as novel ferroelectric phases. Given the high Curie temperature of the Aurivillius phase thin films (T_c generally over 500 °C),[45,46] potential commercial applications of BTF7M3O and BTF7C3O thin films include lead-free piezoelectrics for adverse environments, components in ferroelectric random access memories and tunnel junctions, and high density data storage by ferroelectric lithography.

[1]D. N. Astrov, Sov. Phys. JETP **11**, 708 (1960).
[2]S. Dong, J.-F. Li, and D. Viehland, Appl. Phys. Lett. **83**(11), 2265–2267 (2003).
[3]W. Eerenstein, N. D. Mathur, and J. F. Scott, Nature **442**(7104), 759–765 (2006).
[4]*International Technology Roadmap For Semiconductors*, 2009 Edition, Emerging Research Materials.
[5]E. Ascher, H. Rieder, H. Schmid, and H. Stossel, J. Appl. Phys. **37**(3), 1404–1405 (1966).
[6]G. Catalan and J. F. Scott, Adv. Mater. **21**(24), 2463–2485 (2009).
[7]B. Aurivillius, Ark. Kemi **1**, 499 (1949).
[8]S. Patri, R. Choudhary, and B. Samantaray, J. Electroceram. **20**(2), 119–126 (2008).
[9]R. A. Armstrong and R. E. Newnham, Mater. Res. Bull. **7**(10), 1025–1034 (1972).
[10]P. Boullay, G. Trolliard, D. Mercurio, J. M. Perez-Mato, and L. Elcoro, J. Solid State Chem. **164**(2), 252–260 (2002).
[11]S.-l. Ahn, Y. Noguchi, M. Miyayama, and T. Kudo, Mater. Res. Bull. **35**(6), 825–834 (2000).
[12]Y. Noguchi, K. Yamamoto, Y. Kitanaka, and M. Miyayama, J. Eur. Ceram. Soc. **27**(13–15), 4081–4084 (2007).
[13]N. A. Hill, J. Phys. Chem. B **104**(29), 6694–6709 (2000).
[14]N. A. Lomanova, M. I. Morozov, V. L. Ugolkov, and V. V. Gusarov, Inorg. Mater. **42**, 189 (2006).
[15]X. Y. Mao, W. Wang, and X. B. Chen, Solid State Commun. **147**(5–6), 186–189 (2008).
[16]S. V. Kalinin and A. L. Kholkin, *Preface to Special Topic: Piezoresponse Force Microscopy and Nanoscale Phenomena in Polar Materials* (AIP, 2011).
[17]S. V. Kalinin, N. Setter, and A. L. Kholkin, J. Appl. Phys. **108**(4), 041901 (2010).
[18]L. Keeney, P. F. Zhang, C. Groh, M. E. Pemble, and R. W. Whatmore, J. Appl. Phys. **108**(4), 042004 (2010).
[19]L. Keeney, C. Groh, S. Kulkarni, S. Roy, M. E. Pemble, and R. W. Whatmore, J. Appl. Phys. **112**, 024101 (2012).

[20]J. B. Sun, J. Qu, W. Wang, H. X. Lu, and X. B. Chen, Ferroelectrics **385**, 27–32 (2009).

[21]X. Mao, W. Wang, X. Chen, and Y. Lu, Appl. Phys. Lett. **95**(8), 082901 (2009).

[22]F. Maccherozzi, *PEEM Image Microscopy Manipulation (PIMMs) IGOR routine*.

[23]B. J. Rodriguez, C. Callahan, S. V. Kalinin, and R. Proksch, Nanotechnology **18**(47), 475504 (2007).

[24]S. Jesse, A. Baddorf, and S. Kalinin, Appl. Phys. Lett. **88**(6), 062908 (2006).

[25]S. Jesse, H. N. Lee, and S. V. Kalinin, Rev. Sci. Instrum. **77**(7), 073702 (2006).

[26]S. Jesse, B. J. Rodriguez, A. P. Baddorf, S. V. Kalinin, and M. Alexe, Microsc. Microanal. **13**(suppl. S02), 1582–1583 (2007).

[27]Q. Tian, X. Wang, C. Yu, H. Jiang, Z. Zhang, Y. Wang, and S. Lin, Sci. China, Ser. E **52**(8), 2295–2301 (2009).

[28]F. Yiting, F. Shiji, S. Renying, and M. Ishii, Prog. Cryst. Growth Charact. Mater. **40**(1–4), 183–188 (2000).

[29]Z. G. Zhang, X. F. Wang, and Q. Q. Tian, Sci. Sintering **42**, 51–59 (2010).

[30]V. P. Zhereb and V. M. Skorikov, Inorg. Mater. **39**(0), S121–S145 (2003).

[31]N. Balke, I. Bdikin, S. V. Kalinin, and A. L. Kholkin, J. Am. Ceram. Soc. **92**(8), 1629–1647 (2009).

[32]D. A. Bonnell, S. V. Kalinin, A. L. Kholkin, and A. Gruverman, MRS Bull. **34**(9), 648–657 (2009).

[33]A. Gruverman and S. Kalinin, J. Mater. Sci. **41**(1), 107–116 (2006).

[34]S. V. Kalinin, N. Setter, and A. L. Kholkin, MRS Bull. **34**(9), 634–642 (2009).

[35]T. Watanabe and H. Funakubo, J. Appl. Phys. **100**(5), 051602 (2006).

[36]S. V. Kalinin, A. Gruverman, and D. A. Bonnell, Appl. Phys. Lett. **85**(5), 795–797 (2004).

[37]X.-M. Liu, S.-Y. Fu, and L.-P. Zhu, J. Solid State Chem. **180**(2), 461–466 (2007).

[38]K. Srinivasa Rao, A. Mahesh Kumar, M. Chaitanya Varma, G. S. V. R. K. Choudary, and K. H. Rao, J. Alloys Compd. **488**, L6–L9 (2009).

[39]B. D. Cullity, *Elements of X-Ray Diffraction*, 2nd ed. (Addison-Wesley, 1978).

[40]Crystallographica, v1.60d, (c) Oxford Cryosystems Ltd., 1995-2007.

[41]C. H. Hervoches, A. Snedden, R. Riggs, S. H. Kilcoyne, P. Manuel, and P. Lightfoot, J. Solid State Chem. **164**, 280–291 (2002).

[42]M. E. Fleet, J. Solid State Chem. **62**(1), 75–82 (1986).

[43]V. L. Mazzocchi and C. B. R. Parente, J. Appl. Crystallogr. **31**(718), 718–725 (1998).

[44]H. E. Swanson, H. F. McMurdie, M. C. Morris, E. H. Evans, and B. Par-etzkin, Natl. Bur. Stand (U.S.) Monogr. **25**(9), 22 (1971).

[45]A. Moure, A. Castro, and L. Pardo, Prog. Solid State Chem. **37**(1), 15–39 (2009).

[46]J. Wang *et al.*, Chin. Phys. Lett. **26**(11), 117301 (2009).